Enhancement of H2 and light oil production and CO2 emission mitigation during co-pyrolysis of oily sludge and incineration fly ash

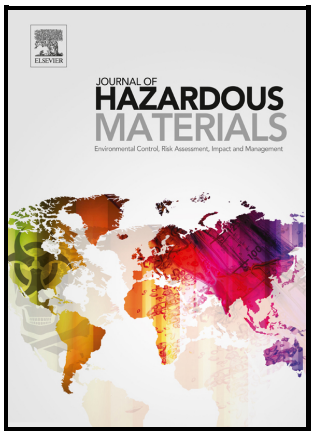

Di Yu, Zhiwei Li, Jie Li, Jun He, Bo Li, Yin Wang

PII: S0304-3894(23)01901-5

DOI: https://doi.org/10.1016/j.jhazmat.2023.132618

Reference: HAZMAT132618

To appear in: *Journal of Hazardous Materials*

Received date: 3 July 2023
Revised date: 4 September 2023
Accepted date: 22 September 2023

Please cite this article as: Di Yu, Zhiwei Li, Jie Li, Jun He, Bo Li and Yin Wang, Enhancement of H2 and light oil production and CO2 emission mitigation during co-pyrolysis of oily sludge and incineration fly ash, *Journal of Hazardous Materials,* (2023) doi:https://doi.org/10.1016/j.jhazmat.2023.132618

Enhancement of H_2 and light oil production and CO_2 emission mitigation during co-pyrolysis of oily sludge and incineration fly ash

Di Yu[1, 2, 3], Zhiwei Li[1], Jie Li[1], Jun He[3, 5], Bo Li[2, *], Yin Wang[1, 4, *]

1 *Key Laboratory of Urban Pollutant Conversion, Institute of Urban Environment, Chinese Academy of Sciences, Xiamen 361021, China.*

2 Department of Civil Engineering, University of Nottingham Ningbo China, Ningbo 315100, China.

3 Department of Chemical and Environmental Engineering, University of Nottingham Ningbo China, Ningbo 315100, China.

4 Zhejiang Key Laboratory of Urban Environmental Processes and Pollution Control, CAS Haixi Industrial Technology Innovation Center in Beilun, Ningbo 315830, China.

5 Nottingham Ningbo China Beacons of Excellence Research and Innovation Institute, Ningbo 315100, China.

** Corresponding authors:*

E-mail address: yinwang@iue.ac.cn; bo.li@nottingham.edu.cn

Abstract

The proper treatment and utilization of oily sludge (OS) and incineration fly ash (IFA) remains a significant challenge due to their hazardous nature. To attain effective recovery of petroleum hydrocarbons and synergistic disposal, this study investigated the co-pyrolysis of OS and IFA, resulting in successful energy recovery, CO_2 mitigation, and heavy metal immobilization. Results revealed that the peak ratio of light oil to heavy oil fractions reached 179.42% with 20 wt% IFA addition, accompanied by the highest aromatic hydrocarbons selectivity of 30.72% and the lowest coke yield of 106.13 mg/g OS under the optimal temperature of 600°C. In-depth analysis indicated that IFA inhibited the poly-condensation of macromolecular PAHs and promoted their cracking into light aromatic hydrocarbons. The addition of 50 wt% IFA significantly increased H_2 yield (21.02 L/kg OS to 60.95 L/kg OS) and facilitated CO_2 sequestration due to its higher content of Ca-bearing minerals. Moreover, high IFA ratios promoted the reduction of Fe species in OS to a low-valence state. Heavy metals in co-pyrolysis char were well immobilized into stable fractions with lower environmental risks. This work highlights the potential of co-pyrolysis as a viable approach for simultaneous disposal of multiple hazardous wastes

and offers new insights for their utilization.

Keywords:

Co-pyrolysis, incineration fly ash, oily sludge, oil upcycling, heavy metal stabilization.

1. Introduction

The exploitation, transportation, and refinement of crude oil generate a large amount of oily sludge (OS), which is a complex mixture of petroleum, water, and minerals [12, 47]. Due to its high content of toxic petroleum hydrocarbons, N, S, Cl, and heavy metals (HMs), OS has been classified as a hazardous waste in many countries [12, 19, 51]. Inappropriate disposal can lead to severe environmental pollution. Despite its toxic and carcinogenic properties, the abundant petroleum hydrocarbons in OS makes it a valuable resource for energy recovery [40, 63]. Over the years, various treatment methods such as landfilling [18], incineration [77], solidification/stabilization [23] have been employed to reduce or eliminate hazardous components in OS and mitigate its environmental impact. To recover the oil content, advanced methods have been also developed, including solvent extraction [81], centrifugation [20], freezing [38], surfactant [43], froth flotation [53], ultrasonic irradiation [74], and pyrolysis [13, 22]. Among them, pyrolysis is gaining popularity due to its less chemical consumption, higher energy recovery rate, and lower secondary environmental pollution.

The impacts of pyrolysis parameters (e.g., final temperature, heating rate, retention time) on the distribution and quality of pyrolysis products have been extensively studied [22]. Effective catalyst is critical for improving pyrolysis products [37], and different metal materials have been evaluated for their catalytic impact on OS pyrolysis [15]. Compounds containing calcium can destabilize chemical bonds and accelerate the devolatilization of organics [17, 34, 40]. Fe_2O_3 is an effective oxidizing agent that can break the C-H and C-C bonds of aliphatic hydrocarbons due to its active 2p orbitals [15]. Al_2O_3 could improve the conversion and reaction rate of organic substances in OS [30]. Despite these benefits, the accumulation of coke on catalyst surface can lead to inactivation and a waste of resources [76], which highlights the need for more affordable alternatives. The replacement of metal oxides by solid wastes can reduce resource consumption. However, only few studies have been devoted to investigating the catalytic effect of solid wastes such as red mud, sewage sludge fly ash, OS ash etc., on OS pyrolysis [8, 12, 40].

Various types of catalysts, including traditional alkali and transition metal catalysts, as well as waste-

based catalysts, have been found to be effective in facilitating the simultaneous generation of H_2 and CO_2 during the pyrolysis process [12, 31]. However, it is necessary to reduce CO_2 emissions to produce H_2-rich syngas with high flammability. Despite attempts to optimize operational parameters, minimizing CO_2 emissions and improving the quality of syngas for higher flammability remains a significant challenge [29, 31, 32].

Incineration fly ash (IFA) of municipal solid waste is considered a hazardous waste worldwide due to its toxic composition which includes chlorides, HMs, and polychlorinated dibenzo-p-dioxins and polychlorinated dibenzofurans (PCDD/Fs) [45]. It is primarily composed of Ca-bearing minerals and chlorides, with CaO, $Ca(OH)_2$, $CaCO_3$, and CaClOH [45, 75]. The rich Ca-bearing components and alkali chlorides in IFA could provide binding sites for chain scission of organic compounds in OS to yield light hydrocarbons [17, 22] and simultaneously capture CO_2 and H_2S [26, 45]. However, despite its high alkali earth metal content, IFA has rarely been studied as a catalyst for pyrolysis due to the difficulty in its detoxification.

In addition, HM pollution is a prevalent issue in both IFA and OS treatments. The presence of high levels of HMs such as Zn, Pb, Cu, Cd, Cr, and Ni in IFA poses a severe risk to both the environment and human health [65]. HMs in OS would migrate and distribute in the resulting products during pyrolysis, causing a long-term bioaccumulation and biomagnification effect [62]. However, many studies mainly focused on recovering high-grade products during the treatment of multiple hazardous wastes but ignored the evaluation of HM risk assessment of the received products [8, 40]. Therefore, it is essential to investigate the ecological risk of HMs in both IFA and OS after the co-pyrolysis treatment.

Although both OS and IFA have been studied individually, the co-treatment of the two waste streams has not been explored yet in the literature. Therefore, this study aims to develop a co-pyrolysis treatment method for IFA and OS, which can achieve simultaneous improvement in pyrolysis oil and gas quality with the immobilization of HMs. A comparative study of OS pyrolysis with and without IFA addition was carried out at different pyrolysis temperatures to study the catalytic performance of IFA. The effects of the OS/IFA mass ratio on the distribution and quality of pyrolysis products were emphatically investigated at 600ºC. Additionally, an assessment of the environmental risk associated with the pyrolysis chars was performed by comparing leaching toxicity and investigating the speciation transformation of HMs. The study also proposes potential underlying mechanisms responsible for the observed effects and the synergies between OS and IFA. This research presents a feasible and environmentally friendly

solution for the collaborative treatment of two hazardous wastes, simultaneously achieving resource recovery through waste utilization. This approach aligns with industrial sustainability and resource recovery objectives.

2. Materials and methods

2.1. Materials

The oily sludge was provided by Ningbo Haijing Environmental Protection Technology Co., Ltd, which is dark and slimy. The municipal solid waste incineration fly ash was provided by Everbright Environmental Energy (Ningbo) Co., Ltd., and it is in the form of fine white powdery particles and exhibits no agglomeration. Both IFA and OS were heated at 105°C for 12h in an oven before being individually blended to ensure homogeneity. They were then stored in a rapid glass dryer until further use. Proximate and ultimate analysis were performed for both OS and IFA, and the results are listed in Table 1. The proximate analysis was determined by a muffle according to the Chinese standard GB/T 212-2008 (Proximate analysis of coal), and the ultimate analysis was determined by element analyzer (Vario MAX, Germany). The minerals detected in IFA and OS solid fraction according to X-ray Diffraction (X'Pert Pro, Netherlands) are present in Fig. S1, and the element compositions of both IFA and solid fraction of OS were detected by X-ray Fluorescence (Axios-MAX, Netherlands) as shown in Table 2. The higher heating value (HHV) of the oily sludge was measured using the oxygen bomb calorimeter (XRY-1A+, China), and its value is 18.02 MJ/kg, which is close to that of coal (17.4-23.9 MJ/kg). The oil content (30.43wt%) and solid content (52.26wt%) are defined based on ASTM D95-13 [21]. Additionally, the average pore diameter of IFA was determined by Brunauer–Emmett–Teller (BET) analysis. To ensure reproducibility, all tests were repeated at least three times under the same operation conditions.

The addition ratios of IFA were set at 0, 10, 20, 30, and 50wt% to study its effect on the co-pyrolysis of IFA and OS. The IFA and OS were mixed in different proportions and were stirred for 10 min to ensure uniformity. The feedstocks were labeled as OS and IFA respectively, and the pyrolysis products produced under different pyrolysis conditions were labeled as Mixture-T, where Mixture stands for the IFA addition weight ratio and T represents the final pyrolysis temperature. For example, 50IFA-600 represents the pyrolysis products obtained from the pyrolysis of OS with 50wt% IFA addition at 600°C, and OS-400 represents the pyrolysis products obtained from the pyrolysis of OS at 400°C.

Table 1 Primary components of OS and IFA (M: moisture, A: ash; V: volatile; FC: fixed carbon; a: as received; b: dry basis; O was calculated through O%=100-C%-H%-N%-ash%).

Material	Proximate analysis (wt.%)				Ultimate analysis (wt.%)					Oil content (wt.%)	Solid content (wt.%)
	M^a	A^b	V^b	FC^b	C	H	O	N	S		
OS	17.31	48.28	38.89	12.83	38.28	4.52	20.03	0.38	9.24	30.43	52.26
IFA	2.59	82.50	17.26	0.24	2.80	1.78	12.50	0.43	2.79	/	/

Table 2 Elemental composition of IFA and OS solid fraction detected by XRF (on dry basis).

	Mineral contents (wt%)									
	CaO	Fe_2O_3	Al_2O_3	Na_2O	K_2O	SiO_2	MgO	ZnO	Cl	SO_3
OS	14.83	24.41	11.80	0.55	0.15	12.52	0.63	0.35	0.15	22.27
IFA	52.73	0.45	0.38	10.55	3.86	1.62	0.69	0.57	20.96	7.47
	PbO	TiO_2	CuO	SrO	Sb_2O_3	BaO	Cr_2O_3			
OS	0.02	0.29	0.21	0.03	0.03	0.31	/			
IFA	0.16	0.11	0.07	0.03	0.03	0.03	0.03			

2.2. Experimental apparatus and methods

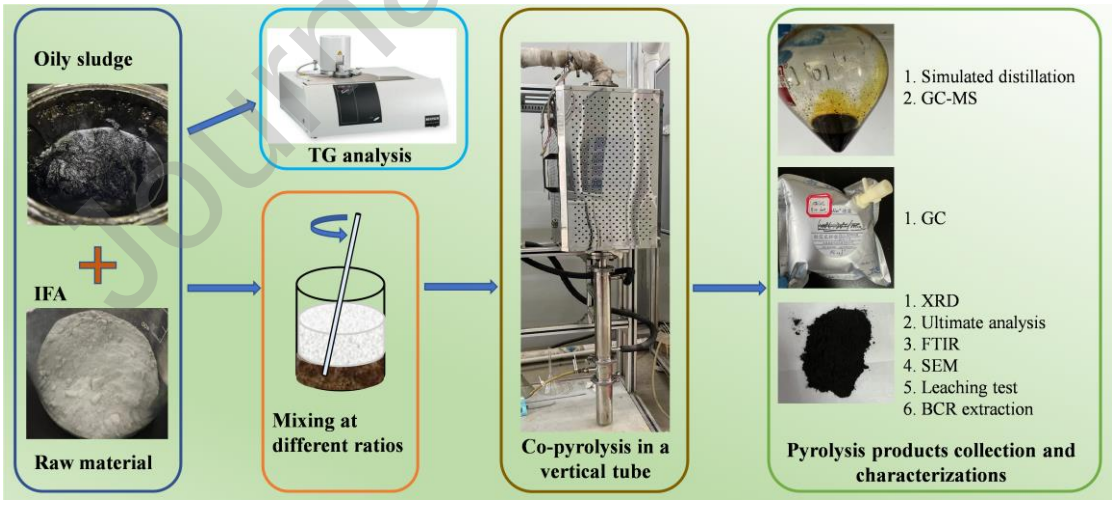

Fig. 1 Schematic diagram of co-pyrolysis of OS with IFA.

2.2.1 TG and DTG analysis

The thermogravimetric and derivative thermogravimetric (TG-DTG) analyses were conducted on a thermogravimetric analyzer (Netzsch TG 209 F3, Germany). To reduce experimental error before

thermogravimetric experiments, a thermogravimetry baseline was established. 40-50 mg of the sample was loaded into the TG reactor and then was heated from 40°C to 800°C purging with 99.999% pure nitrogen at a heating rate of 10 °C min^{-1}. A flow rate of 60 mL min^{-1} was adopted to blow away non-condensable gas products.

2.2.2 Pyrolysis

The pyrolysis experiments were carried out in a vertical pyrolysis apparatus as shown in Fig. S2. The raw materials, including OS, IFA, and their mixtures, with a total mass of 50 g were placed in a stainless-steel tube over the sieve plate. High purity N_2 was continuously supplied from the top of the reactor at a flow rate of 200 ml min^{-1} to drive away the air in the reactor and create an inert atmosphere for 30 minutes, and then it would be lowered to 150 ml min^{-1}. The samples were heated to the targeted temperatures (e.g., 400, 500, and 600°C) with a heating rate of 10 °C min^{-1} for 60 min for heat preservation. The condenser was set to be -10 °C for the condensation of pyrolysis oil, and 3 bottles of acetone washing cylinders in ice bath condition were placed as second oil absorbers. After pyrolysis, the condenser and the oil container would be washed with acetone to make sure the complete collection of pyrolysis oil. Adequate magnesium sulfate ($MgSO_4$) was added to the liquid mixture to eliminate the water in the product. Finally, rotary evaporation at 27°C was conducted to extract the pyrolysis oil from the acetone solution, which was then weighed and analyzed to obtain its yield and composition. Afterwards, the non-condensable gas went through a saturated sodium bicarbonate washing bottle and a silica gel washing bottle to eliminate H_2S and water, respectively. The pyrolysis gas was finally collected in a gas bag, and the solid residue in the sample container would be collected to obtain its yield for further analysis.

The investigation of OS pyrolysis product distribution under various IFA additions involved obtaining oil and pyrolysis residue yields through weighing, while gas component mass was deduced through subtraction. It is important to highlight that the mass of added IFA was subtracted from the pyrolysis residue mass to ascertain the char yield of OS, and this adjustment was necessary due to the in-situ blending of OS with IFA. The oil yield $Y_{oil(daf)}$ (wt%), char yield $Y_{char(daf)}$ (wt%), and gas yield $Y_{g(daf)}$ (wt%) were calculated through the Eqs. (1) to (3).

$$Y_{oil(daf)} = \frac{m_{oil}}{m_{OS}} \times 100\% \quad (1)$$

$$Y_{char(daf)} = \frac{m_{solid\ residue} - m_{IFA} \times (1 - Loss_{IFA}\%)}{m_{OS}} \times 100\% \quad (2)$$

$$Y_{gas(daf)} = 100wt\% - Y_{oil(daf)} - Y_{char(daf)} \quad (3)$$

where m_{OS}, m_{IFA} are the masses of OS and IFA (kg) in the feedstock, m_{oil} and $m_{solid\ residue}$ refer to the masses of pyrolysis oil and solid residue (kg), respectively; As IFA is not totally inert during the pyrolysis with temperature over 400°C, the weight loss percentage of IFA $Loss_{IFA}\%$ after pyrolyzed at certain temperature (4.35wt%-400°C, 7.24wt%-500°C, 8.66wt%-600°C), as shown in Fig. S3, is considered, which is normally ignored in previous studies [12, 40].

The volume yield of each gas component in pyrolysis gas $Y_{gV(daf)}$ was calculated by Eq. (4).

$$Y_{gV(daf)} = \frac{V_{gas(daf)} \times V_j\%}{m_{OS}} \quad (4)$$

where $V_{gas(daf)}$ refers to the pyrolysis gas volume (L) recorded by wet gas meter, $V_j\%$ is the volume ratio of each gas component obtained from GC results.

Simulated distillation GC (SCION 456-GC) was utilized to obtain the boiling point distribution of pyrolysis oil according to ASTM D2887 which classify the pyrolysis oil into four different commercial oil products, including Gasoline (<180°C), Diesel (180°C~350°C), Distillates (350°C~500°C), and Heavy oil (>500°C) [14]. The yield of each oil fraction $Y_{D(daf)}$ (wt%) can be defined as Eq. (5).

$$Y_{D(daf)} = Y_{oil(daf)} \times m_i\% \quad (5)$$

where $m_i\%$ is the weight ratio of gasoline, diesel, distillates, and heavy oil in the total oil.

GC/MS (Agilent 7890A/5975C) was applied to obtain oil compositions according to the standard spectrum in NIST 05 standard mass spectrogram library.

To obtain the accurate carbon coke yield, hydrochloric acid (2 mol/L) was utilized to wash and remove the carbonates in pyrolysis char [4, 48, 56]. Afterwards, $C_{TOC(daf)}$ (mg/g washed residue) referred to the carbon content in residue after acid washing was measured by element analyzer. The carbon coke content $C_{coke(daf)}$ (mg/g solid residue) can be calculated by Eq. (6) and then could be converted into $Y_{coke(daf)}$ (mg/g OS) by Eq. (7). The total carbon content in chars $C_{TC(daf)}$ (mg/g solid residue) was measured by element analyzer. The eliminated inorganic carbon content (IC) $C_{IC(daf)}$ (mg/g solid residue) during acid washing could be calculated by Eq. (8) [48], and it was mostly in the form of carbonates. The proximate amount of CO_2 adsorbed in char $A_{CO_2(daf)}$ (mg/g solid residue) can be then calculated by Eq. (9), and the disturbance of inherent $CaCO_3$ in IFA $A_{CO_2(IFA)}$ (mg/g solid residue) can be quantified by Eq. (10). The inherent $CaCO_3$ concentration in the raw IFA $CaCO_3\%$ was determined by TG results of $CaCO_3$ and IFA [55, 58], as shown in Fig. S4, according to Eq. (11), and the result is 17.17 %.

$$C_{coke(daf)} = \frac{C_{TOC(daf)} \times m_{washed\ residue}}{m_{solid\ residue}} \quad (6)$$

$$Y_{coke(daf)} = Y_{coke(daf)} * \frac{m_{solid\ residue}}{m_{OS}} \quad (7)$$

$$C_{IC(daf)} = C_{TC(daf)} - C_{coke(daf)} \quad (8)$$

$$A_{CO_2(daf)} = \frac{C_{IC(daf)}}{M_{Carbon}} \times M_{CO_2} - A_{CO_2(IFA)} \quad (9)$$

$$A_{CO_2(IFA)} = \frac{CaCO_3\% \times m_{IFA}}{m_{solid\ residue}} \times \frac{M_{CO_2}}{M_{CaCO_3}} \quad (10)$$

$$CaCO_3\% = 100\% \times \frac{Mass\ loss_{IFA}}{Mass\ loss_{CaCO_3}} \quad (11)$$

where $m_{washed\ residue}$ is the mass of residue after HCl washing; M_{Carbon}, M_{CO_2}, and M_{CaCO_3} refer to the molar mass of carbon, carbon dioxide, and calcium carbonate, which are 12 g/mol, 44 g/mol, and 100 g/mol, respectively; $Mass\ loss_{IFA}$ and $Mass\ loss_{CaCO_3}$ refer to the mass loss of IFA and $CaCO_3$ within 600-810°C by TG, respectively [57].

Fourier Transform Infrared Spectroscopy (FTIR) and scanning electron microscopy (SEM) were employed to analyze the functional groups present in the chars and examine the microstructure of the raw materials as well as the pyrolysis chars.

2.3 Methods for HMs analysis

The total concentrations of HMs were measured after digestion in an acid mixture (HNO_3: HF: $HClO_4$: =3:1:1, v/v/v) [7] and passing through a 0.45 μm membrane filters before being diluted to a constant volume with 2% HNO_3 and detected by Inductively Coupled Plasma Mass Spectrometry (ICP-MS, 7700) and Inductively Coupled Plasma Optical Emission Spectroscopy (ICP-OES, ULTIMA 2).

The toxicity characteristic leaching procedure (TCLP) and modified European Community Bureau of Reference (BCR) sequential extraction method were applied to evaluate the leaching risks and chemical speciation of HMs in OS, IFA, and their pyrolysis chars. The TCLP leachate was extracted using a solution of glacial acetic acid (pH 2.88) at a liquid-to-solid ratio of 20:1. The extraction process was performed in a shaking incubator at 200 r·min^{-1} for 18 hours. Afterwards, the liquid phase was separated by centrifugation at 4000 r·min^{-1}, and the resulting supernatant was filtered through a 0.45 μm membrane. The filtered solution was then analyzed using ICP-MS and ICP-OES [7]. The extraction of acid soluble/exchangeable fraction (F1), reducible fraction (F2), and oxidizable fraction (F3) was referred to

Baig et al. [2]. The residual fraction (F4) was obtained by the difference between the total HM content and the other three fractions. Three parallel samples are set for ensuring the validity of the experimental data.

The potential ecological risk index (RI) was calculated to evaluate the environmental risk of HMs according to Eqs. (12) and (13) [7, 67]:

$$E_r = T_r \times C_f = T_r \times (C_1 + C_2 + C_3)/C_4 \quad (12)$$

$$RI = \sum E_r \quad (13)$$

where RI represents the potential ecological risk index of the samples by adding up each HM's potential ecological index; E_r is the potential ecological risk factor for each HM element; T_r is the toxic factor of the individual HMs, including Cd (30), Cr (2), Cu (5), Ni (6), Pb (5), and Zn (1) [7, 33]; C_f is the contamination factor of an individual HM; C_1, C_2, C_3, and C_4 corresponds to the concentrations of F1, F2, F3, and F4 fractions of the HMs, respectively. The ecological risk assessment, including the indices C_f, E_r and RI [10], is presented in Table S1.

Theoretical values for total heavy metal content (mg/kg solid residue), heavy metal leaching concentration (mg/L), and concentrations of F1, F2, F3, and F4 fractions (mg/kg solid residue) in co-pyrolysis chars (50IFA-T), denoted as C_{T-theo}, are calculated using data obtained from individual pyrolysis of OS and IFA at different temperatures, as shown in Eq. (14). Additionally, the yield of solid fraction (wt%) after individual pyrolysis of OS and IFA, represented as $Y_{s(daf)}$, is also considered according to Eq. (15). By comparing these theoretical values with the experimental results, the impact of co-pyrolysis on the migration and stabilization characteristics of HMs in OS and IFA could be identified.

$$C_{T-theo-co} = \frac{C_{T-IFA} \times Y_{s(IFA-T)} + C_{T-OS} \times Y_{s(OS-T)}}{Y_{s(IFA-T)} + Y_{s(OS-T)}} \quad (14)$$

$$Y_{s(daf)} = \frac{m_{solid\ residue}}{m_{feedstock}} \times 100\% \quad (15)$$

where C_{T-IFA} and C_{T-OS} are the experimental total/leaching/F1-F4 concentrations of IFA and OS at specific temperature, respectively; $m_{feedstock}$ refers to the mass of OS or IFA (kg) during their individual pyrolysis.

3. Results and Discussion

3.1 Effect of pyrolysis temperature on OS pyrolysis with and without IFA addition

Fig. 2(a) presents the thermal characteristics of OS and IFA based on TG analysis. The three peaks at

temperatures of 149°C, 401°C, and 748°C in the DTG curves demonstrate that OS decomposition could be divided into 3 phases. The initial phase (PH1) is attributed to the devolatilization of water and some light hydrocarbons, ranging from 90-182°C. The second phase (PH2) ranging from 182-513°C involves the thermal decomposition and devolatilization of petroleum hydrocarbons, including those with higher boiling points. The last phase (PH3) ranging from 600°C-770°C is mostly due to the decomposition of inorganic minerals [41]. The residual mass at 800°C is approximately 56.93%, which is consistent with the high solid content in OS as shown in Table 1. IFA exhibits a negligible mass loss below 350°C. However, significant weight losses occur in two distinct temperature ranges, including 350°C-500°C and 600°C-810°C, which are derived from the decomposition of $Ca(OH)_2$ and $CaCO_3$ [25], as indicated in Fig. S4.

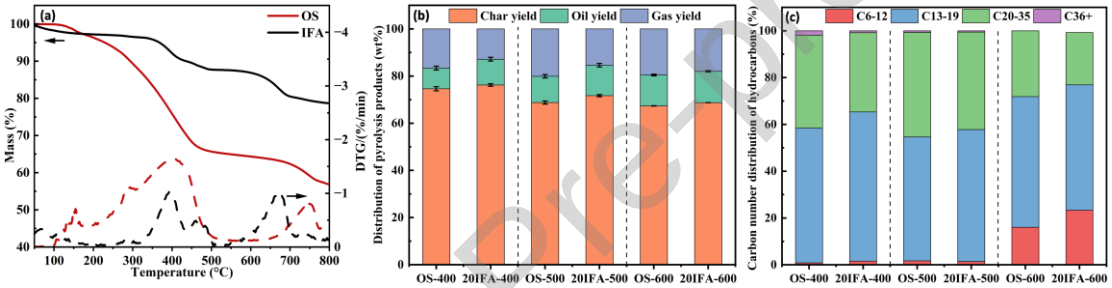

Fig. 2 (a) TG and DTG curves of individual pyrolysis of OS and IFA from 50-800°C; (b) weight distribution of pyrolysis products, and (c) carbon number distributions of hydrocarbons in pyrolysis oil during the pyrolysis of OS with and without 20wt% IFA addition under different final pyrolysis temperatures (400, 500, and 600°C).

Pyrolysis temperature has a significant effect on pyrolysis oil yield and quality. As depicted in Fig. 2(a), the conversion of organics in OS is nearly complete around 513°C. Notably, $CaCO_3$ degradation, causing CO_2 release and potential gas quality deterioration, predominantly transpires beyond 600°C (Fig. S4). These elevated temperatures also entail substantial energy consumption. Therefore, pyrolysis temperatures of 400, 500, and 600°C were adopted in this study. The IFA ratio was fixed as 20% by mass, as it is situated in the middle range and sufficiently high to elicit a catalytic effect. The impacts of final temperatures on the product distribution and oil compositions of OS pyrolysis with and without IFA addition are illustrated in Figs. 2(b) and 2(c), respectively. The simultaneous decrease in char yield and increase in oil yield with increased temperature demonstrate that the elevating temperature promoted thermal conversion of organic matter from solid to oil fractions. Moreover, a significant increase in oil

yield was observed at 400 and 500°C with the addition of IFA, indicating the strong catalytic effects of IFA on accelerating the thermal decomposition of OS at a lower temperature. Interestingly, the addition of IFA also increased char yield, but decreased the gas yield. This tendency was rarely reported in the literature of catalytic pyrolysis, as the increase in oil and gas yield is normally contributed by enhanced volatilization and decomposition of heavy components attached in solid fractions [12, 22, 40]. This phenomenon could be attributed to CO_2 and H_2S adsorption by Ca-bearing minerals in IFA, which will be further discussed in section 3.4.2. At 600°C, the highest oil yield (i.e., 13.30wt%) was observed with 20wt% IFA addition.

The obtained carbon number distribution of hydrocarbons in pyrolysis oil from GC-MS results suggest that increasing the temperature from 400°C to 500°C decreased the content of C13-19 but increased the content of C20-C35, which can be attributed to the enhanced devolatilization of heavy oil components at 500°C. However, the content of C6-C12 increased dramatically when the temperature was raised to 600°C, which suggests that heavy components underwent further cracking at 600°C. On the other hand, the addition of IFA increased the content of C6-C19 at each pyrolysis temperature, indicating its capacity of promoting the decomposition of heavy oil components and improving oil quality. At 600°C, the proportion of C6-12 fractions increased by 7.34% with 20wt% IFA addition. Therefore, 600°C was selected as the optimal temperature for the subsequent experiments to achieve the highest oil recovery rate with better oil quality.

3.2 OS pyrolysis with different IFA addition ratios

The effects of IFA addition ratios on the yields of pyrolysis oil, gas, and char at 600°C are presented in Fig. 3(a). The char yield increased from 67.34wt% to 68.70wt% when the IFA addition ratio increased from 0 to 20wt%. However, it changed marginally when the IFA addition ratio further increased. The sample 30IFA-600 achieved the maximum oil yield of 14.41wt%, while adding IFA at other ratios also increased the oil yield to a lesser extent. The decreased gas yield with the addition of IFA could be attributed to the CO_2 adsorption by Ca-based minerals in IFA.

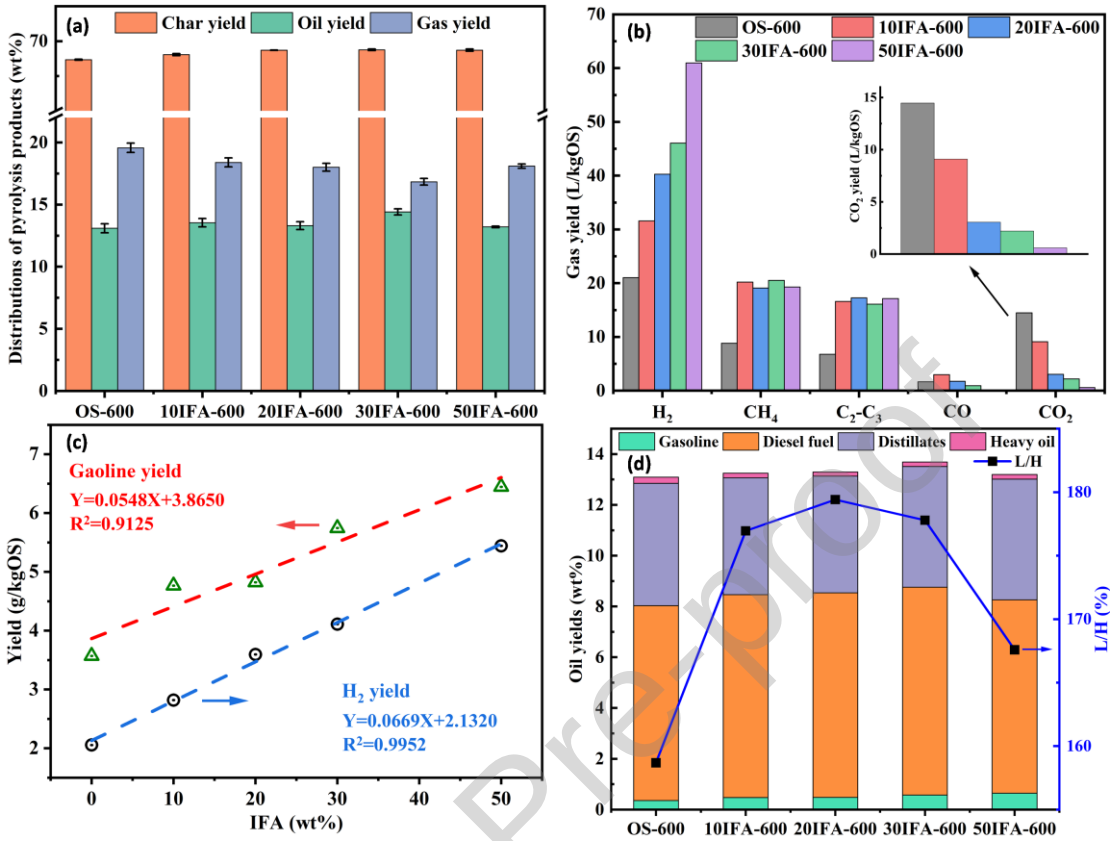

Fig. 3 Effect of IFA addition ratios on (a) pyrolysis products distributions, (b) pyrolysis gas compositions, (c) gasoline and H_2 yields, and (d) the distributions of different oil fractions in pyrolysis oil obtained from the co-pyrolysis at 600°C.

3.2.1 Effect of IFA addition on the compositions of pyrolysis gas from co-pyrolysis with OS

The addition of IFA altered the compositions of OS pyrolysis gas significantly, and the details are presented in Fig. 3(b). H_2 yield increased from 21.02 to 60.95 L/kg OS as the IFA addition ratio increased from 0wt% to 50wt%, which also exhibited a well-fitted linear relationship (R^2=0.9952) as shown in Fig. 3(c). The water-gas shift reaction and dehydrogenation reactions, including cracking of long-chain hydrocarbons, cyclization, polymerization, and aromatization, are dominant reactions for H_2 generation during OS pyrolysis [12, 78]. It is evident that the minerals in IFA promoted some of these reactions. Additionally, the significant increase in H_2 yield with elevated IFA addition ratio (30 wt% to 50 wt%) corresponds to a slight rise in total gas yield shown in Fig. 3(b).

The CO_2 adsorption by Ca-bearing minerals in IFA significantly reduced CO_2 yield from 14.47 to 0.59 L/kg OS with 50wt% IFA addition, achieving the elimination of the non-combustible gas in the content.

On the other hand, the addition of 10wt% IFA increased the CO yield from 1.66 to 2.97 L/kg OS. However, it was decreased as the IFA addition ratio further increased, which may be derived from its consumption through the water-gas shift reaction, as illustrated by Eq. (16) [49]. A sharp increase in CH_4 yield, from 8.84 to 20.20 L/kg OS, was observed with the addition of 10wt% IFA, but it remained constant as the IFA addition ratio further increased. Meanwhile, the content of hydrocarbons with 2-3 carbons presented a similar increased tendency with CH_4 content, which could be attributed to enhanced side chain decomposition of aliphatic compounds [68]. Collectively, the gas products generated during the pyrolysis process contain high levels of energy-rich gases like H_2 and hydrocarbons, while having low levels of CO_2, which makes it a potential fuel in a gas-fired engine to generate energy for the pyrolysis process.

$$CO + H_2O \leftrightarrow CO_2 + H_2 \quad (16)$$

3.2.2 Effect of IFA addition on the compositions of pyrolysis oil from co-pyrolysis with OS

The quality of the oil is determined by its boiling point distribution, and it varied significantly with different IFA addition ratios, as shown in Fig. 3(d). Fig. 3(c) presents a linear correlation between the gasoline yield and the IFA addition ratio (R^2=0.9125). This correlation implies the possibility of enhanced cracking or reforming reactions facilitated by the presence of IFA, potentially leading to a higher selectivity for gasoline within the pyrolysis oil. Diesel was the most abundant component in the pyrolysis oil, which is consistent with Gong et al.'s findings [15], and it increased from 7.67wt% to 8.18wt% when 30wt% IFA was added. Gasoline and diesel are commonly classified as light oil fraction, while distillates and heavy oil are defined as heavy oil fraction. The elevated IFA addition ratios firstly increased light oil fraction from 8.03wt% (OS-600) to 8.76wt% (30IFA-600), and then slightly decreased to 8.27wt% (50IFA-600). Moreover, the adequate addition ratio of IFA (10wt%-30wt%) led to an increase of around 20% in light oil fraction to heavy oil fraction ratio (L/H), and the highest L/H was achieved in 20IFA-600 (179.42%). This demonstrates that a moderate IFA addition ratio could effectively promote light oil formation and improve oil quality. The relatively lower L/H (167.59%) and higher heavy oil yield (4.93wt%) obtained from 50IFA-600 could be attributed to the promotion effect of excessive catalyst on polymerization and condensation [40].

Fig. 4(a) depicts significant changes in pyrolysis oil composition corresponding to varying IFA addition ratios. The cracking and aromatization of middle and long-chain alkanes could be the primary reactions during the co-pyrolysis of IFA and OS, as evidenced by the decrease in straight-chain alkanes of C13-35

and the increase in aromatic hydrocarbons with the addition of IFA. The variation tendency of hydrocarbons in C6-19 aligns with the aromatic hydrocarbons (Fig. 4(b)) when IFA ratio increased, which indicates that the increase in light oil fractions is primarily contributed by the augmented levels of light aromatic hydrocarbons, rather than alkanes (Fig. 4(c)). Moreover, the selectivity of total aromatic hydrocarbons and mono-cyclic aromatic hydrocarbons (MAHs) content in 20IFA-600 increased from 24.63% to 30.72% and from 3.44% to 6.61%, respectively. The corresponding intensity of MAHs, such as phenylethylene and trimethyl-Benzene, are presented in GC-MS result (Fig. S5). Additionally, the destruction of asphaltenes also contributed to the simultaneous increase in polycyclic aromatic hydrocarbons (PAHs) [37], and it is discussed further in subsequent sections. The decrease in the proportion of long and middle-chain alkanes signifies their conversion through cracking into various short-chain aliphatic hydrocarbons and short-chain radicals [71]. This process results in the formation of non-condensable gases, as shown in Fig. 3(b), and subsequently initiates cyclization and aromatization reactions [13]. The long-chain alkanes (C20-35) content slightly increased from 21.83% to 26.95% when the IFA ratio further increased from 20wt% to 50wt%, partially resulting from the polymerization or addition reactions of olefins, as explicated by the corresponding decrease in the proportion of olefins.

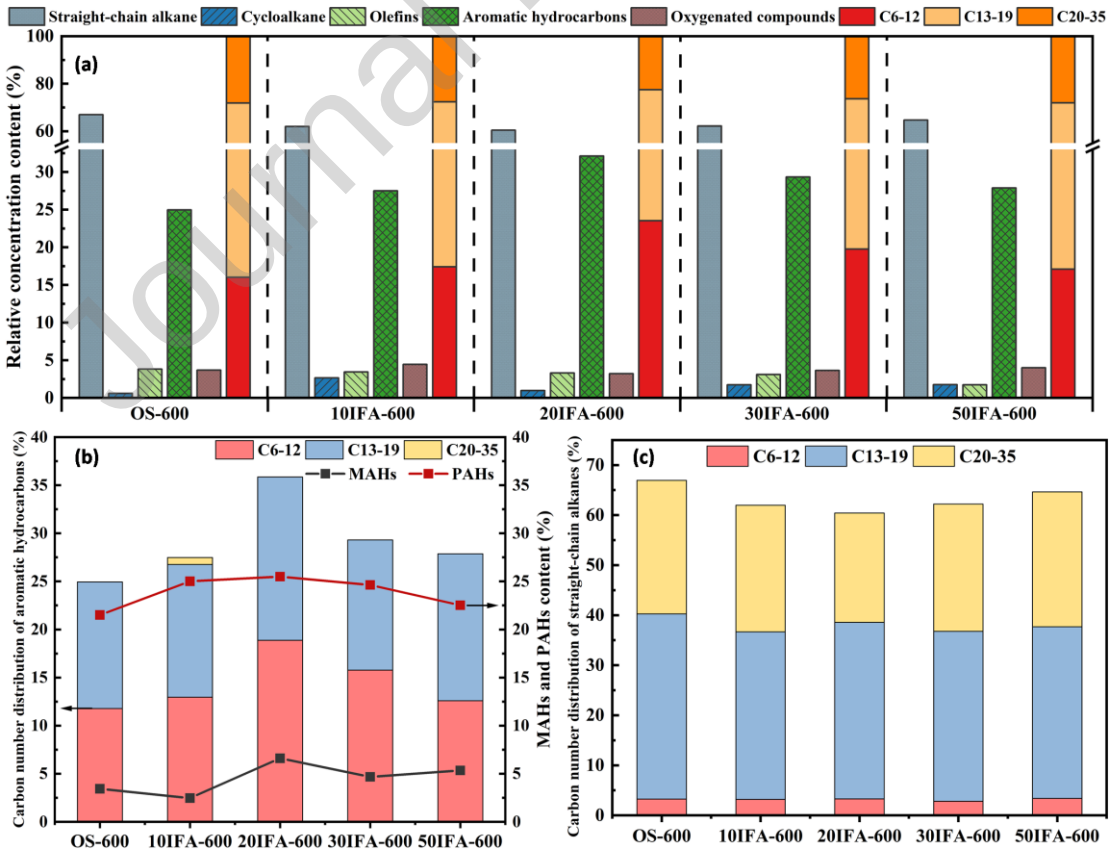

Fig. 4 Effect of IFA addition ratios on (a) the compositions, including relative concentration contents of straight-chain alkanes, cycloalkanes, olefins, aromatic hydrocarbons, oxygenated compounds, and the carbon number distribution of hydrocarbons, (b) carbon number and ring number distributions of aromatic hydrocarbons, and (c) carbon number distribution of straight-chain alkanes of pyrolysis oil obtained at 600°C, detected by GC-MS.

3.2.3 Effect of IFA addition on pyrolysis char from co-pyrolysis with OS

The effects of IFA addition ratio on pyrolysis char composition were investigated, with a focus on carbon coke yield and CO_2 sequestration. Coke content derived from the polymerization and condensation of organic substances [28] is critical for evaluating the carbon migration among the products during co-pyrolysis. The quantification of carbon coke contents in chars with low carbonates content was commonly achieved by elemental analysis [8, 26], TG-DSC [61], and separating CO_2 yield under an oxidizing atmosphere by TG-MS [34]. Here the adsorbed CO_2 in char becomes a disturbance for its quantification and was eliminated by dilute hydrochloric acid washing. As shown in Fig. 5(a), the carbon coke yield first decreased from 129.5 to 106.1 mg/g OS when the IFA addition ratio increased from 0 to 20wt%. However, further elevating IFA addition ratio resulted in a contradictory outcome, and the carbon coke yield reached 128.0 mg/g OS at 50wt% IFA addition. This phenomenon indicates that moderate IFA addition could significantly inhibit the polymerization and condensation reactions of large-molecular compounds and promote their decomposition, which explains the increased light aromatic hydrocarbons in pyrolysis oil.

Fig. 5(b) exhibits the total carbon content, carbon coke content, and the derived amount of CO_2 sequestration in the char. The amount of CO_2 retained in the char increased from 93.59 to 131.89 mg/g char as the IFA addition ratio increased from 10wt% to 30wt%. This observation is consistent with the continuous decrease of CO_2 proportion in pyrolysis gas, and it can be explained by the increased CO_2 adsorption substrate. The slight decrease in CO_2 adsorption amount in 50IFA-600 char was attributed to the reduced OS mixing ratio in the feedstock.

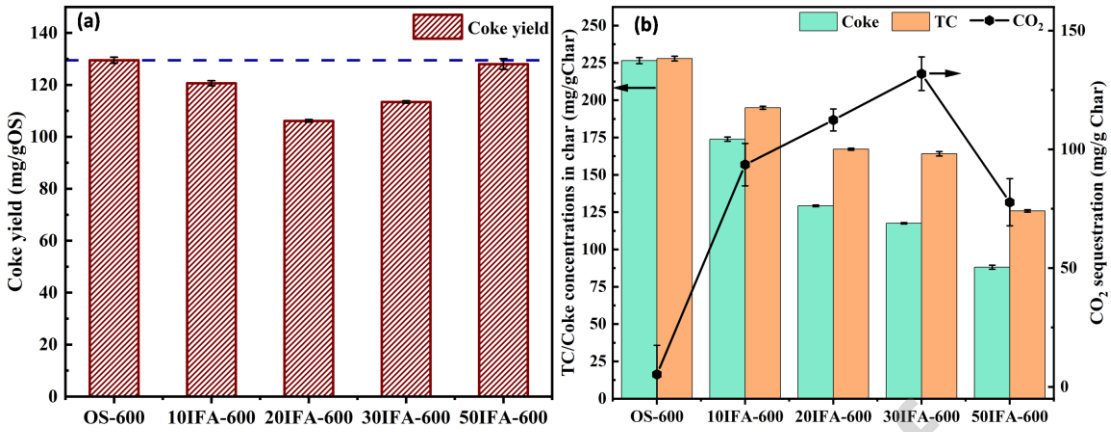

Fig. 5 Effect of IFA addition ratios on the (a) carbon coke yield (mg /g OS), and (b) carbon coke content (mg/g solid residue), total carbon concentration (mg/g solid residue) and the amount of CO_2 sequestration (mg/g solid residue) in solid residues obtained at 600°C.

Microstructural analysis of the feedstock and the derived chars was conducted to analyze the catalytic effect of IFA on co-pyrolysis from a physical catalysis perspective. Fig. S6 reveals that solid particles in the original oily sludge were enveloped by crude oil and clustered into dense formations. After pyrolysis, the OS char's surface adopts a sleek and clustered structure, whereas IFA addition leads to a relatively voluminous and more widely dispersed configuration. The N_2 adsorption-desorption curve (Fig. S7a) of IFA exhibits a hysteresis loop and a type IV isotherm, signifying the presence of mesopores within IFA. Furthermore, Barrett-Joyner-Halenda (BJH) pore size distribution curves (Fig. S7b) indicate mesopores primarily spanning from 2 to 30 nm, centered around 3.8 nm, with an average pore diameter of 11.98 nm. This suggests the presence of potential accessible pathways for transporting medium and large molecular compounds, facilitating catalytic cracking [79].

3.3 Speciation and environmental risk of HMs

To evaluate the effect of pyrolysis temperatures and co-pyrolysis process on the stabilization of HMs in OS and IFA, the individual pyrolysis of IFA at 400, 500, and 600°C was further conducted for comparison.

3.3.1 Total HMs concentrations and leaching toxicity of HMs in OS, IFA, and chars

The total concentrations of Cr, Cu, Ni, Zn, Cd, Pb in OS, IFA, and their pyrolysis chars at different temperatures are presented in Table S2. The highest HM content in OS was Zn (1648.81 mg/kg), followed by Cu (901.81 mg/kg) and Ni (694.87 mg/kg), while only minor concentrations of Cr (102.12 mg/kg)

and Pb (68.19 mg/kg) were detected. These HMs mainly originated from crude oil, drilling fluid, and soil [11]. IFA served as an efficient solid heat transfer medium and catalyst for OS pyrolysis. However, the inclusion of IFA also resulted in increased concerns regarding HM concentration in the resulting chars after co-pyrolysis [42, 72]. Minor concentrations of Cd, Cr, and Ni (82.33, 56.67, and 27.83 mg/kg) were detected in IFA, while the dominant HM elements were Zn, Pb, and Cu with concentrations of 4646.14 mg/kg, 1330.42 mg/kg, and 514.29 mg/kg, respectively. These HMs were enriched in IFA during the process of waste incineration when they were adhered on the surface of IFA due to their considerable high volatility [16]. It is noted that the total HM concentrations in OS pyrolysis chars were higher than those in raw material, which is due to the decomposition of organic matter and the weight loss of volatile fraction.

Considering both IFA and OS contain high levels of HMs, we compared the HM content in chars obtained from individual pyrolysis and co-pyrolysis at a 1:1 mixing ratio to evaluate the potential of co-pyrolysis for HM stabilization. The experimental total Cr, Ni, and Zn concentrations in co-pyrolysis chars are slightly lower than the theoretical value, implying that a small amount of Cr, Ni, and Zn might have migrated to the pyrolysis gas and oil during co-pyrolysis. However, the opposite trend observed for Cu and Pb suggests that the co-pyrolysis process suppressed their volatilization.

Table 3 Leaching concentrations of HMs in OS, IFA, and chars after pyrolysis at different temperatures.

	Element (mg/L)					
Sample	Cd	Cr	Cu	Ni	Pb	Zn
OS	0.06±0.00	ND	ND	0.02±0.00	0.33±0.00	0.11±0.01
OS-400	0.01±0.00	0.01±0.00	0.01±0.00	0.04±0.00	ND	1.19±0.03
OS-500	0.01±0.00	ND	ND	0.87±0.08	0.02±0.00	0.61±0.07
OS-600	0.01±0.00	ND	ND	0.35±0.01	0.03±0.00	1.47±0.10
IFA	ND	0.03±0.00	0.09±0.01	0.01±0.00	8.59±0.39	0.78±0.04
IFA-400	ND	0.18±0.00	0.01±0.00	ND	9.19±0.20	2.89±0.08
IFA-500	ND	ND	ND	ND	16.87±0.11	7.86±0.20
IFA-600	ND	ND	0.01±0.00	ND	5.00±0.04	4.37±0.11
50IFA-400	ND	ND	ND	0.01±0.00	ND	0.21±0.00
50IFA-500	ND	0.01±0.00	ND	ND	ND	0.01±0.00
50IFA-600	ND	ND	ND	ND	0.44±0.00	0.65±0.04
Threshold of GB5085.3-2007	1.00	15.00	100.00	5.00	5.00	100.00
Theoretical leaching concentrations of pyrolysis chars after co-pyrolysis						
50IFA-400-theo	0.01	0.10	0.01	0.02	5.16	2.14
50IFA-500-theo	0.00	0.00	0.00	0.37	9.70	4.77
50IFA-600-theo	0.00	0.00	0.01	0.15	2.86	3.13

ND: Not detected.

Table 3 shows that the leaching concentrations of HMs in IFA, OS, and pyrolysis chars. The leaching concentrations of Pb in IFA exceeded the thresholds of the Chinese national standard (GB 5085.3-2007). After individual pyrolysis of IFA, there was no improvement in leaching concentrations of Pb and Zn, and the leaching concentration of Zn increased significantly. These findings suggest that thermal treatment in a reductive atmosphere may increase the leaching rates of Pb and Zn to varying degrees, leading to higher leaching toxicity of the derived pyrolysis chars. A remarkable reduction in the experimental leaching concentrations of Ni, Pb, and Zn in co-pyrolysis chars was observed compared to the theoretical values. This observation highlights that the co-pyrolysis process substantially mitigated the leaching toxicities of OS and IFA, particularly notable for Ni, Pb, and Zn, with all metal concentrations now falling below the USEPA thresholds. These results indicate that the interactions between IFA and OS during co-pyrolysis may alter the metal speciation, leading to the immobilization of HMs.

3.3.2 Speciation of HMs in OS, IFA, and chars

Chemical speciation analysis of HMs is essential for evaluating the ecological toxicity and bioavailability of HMs [7, 51]. The F1 and F2 fractions are named as active fractions, and the F3 and F4 fractions are named as stable fractions. As depicted in Fig. 6, most HMs were in the stable form in OS, except for Cd having 60.53% in the active fraction. After pyrolysis, there was a significant decrease in the F1 fraction of Cd, while Ni, Pb, and Zn showed substantial increases in their active fractions. Furthermore, the active fractions of Cd, Ni, and Zn increased as the temperature elevated from 400°C to 600°C [60]. IFA, on the other hand, exhibited a different distribution of HMs, with Cd, Cu, Ni, Pb, and Zn exhibiting high proportions of 92.37%, 73.87%, 46.96%, 45.49%, and 77.35%, respectively, in active fractions, which is in line with previous study [7]. Pyrolysis of IFA decreased the active fractions of most HMs, except for Ni, which exhibited a slight increase.

Comparing to the theoretical HM speciation values (Fig. S8), co-pyrolysis process significantly shifted Cd, Cu, and Ni into more stable forms, while the stabilization effect was less obvious for Cr, Pb, and Zn. The transformation of HMs between different fractions was influenced by the pyrolysis temperature and specific HM properties. Overall, as the temperature increased, the active fractions of Cr, Cd and Zn underwent a transformation into more stable fractions [7]. However, the active fractions of Cd still

accounted for significant proportions of 55.89%, 60.04%, and 39.53% in chars obtained at 400, 500, and 600°C, respectively, due to the high F2 fraction in IFA. Cu exhibited a decrease in the F4 fraction with a simultaneous increase in the F3 fraction. Similarly, Ni exhibited a transition from the F4 fraction to the F2 and F1 fractions as the temperatures increased, which is consistent with the observed trends in the OS pyrolysis chars. Moreover, the increased F1 fraction at 600°C aligns with the high Pb leaching concentration. These findings suggest that higher pyrolysis temperature may not benefit the immobilization of all types of HMs [33, 51]. Additionally, significant increases of F3 fractions were observed in Cd, Cr, Cu, Pb, and Zn as the pyrolysis temperature increased.

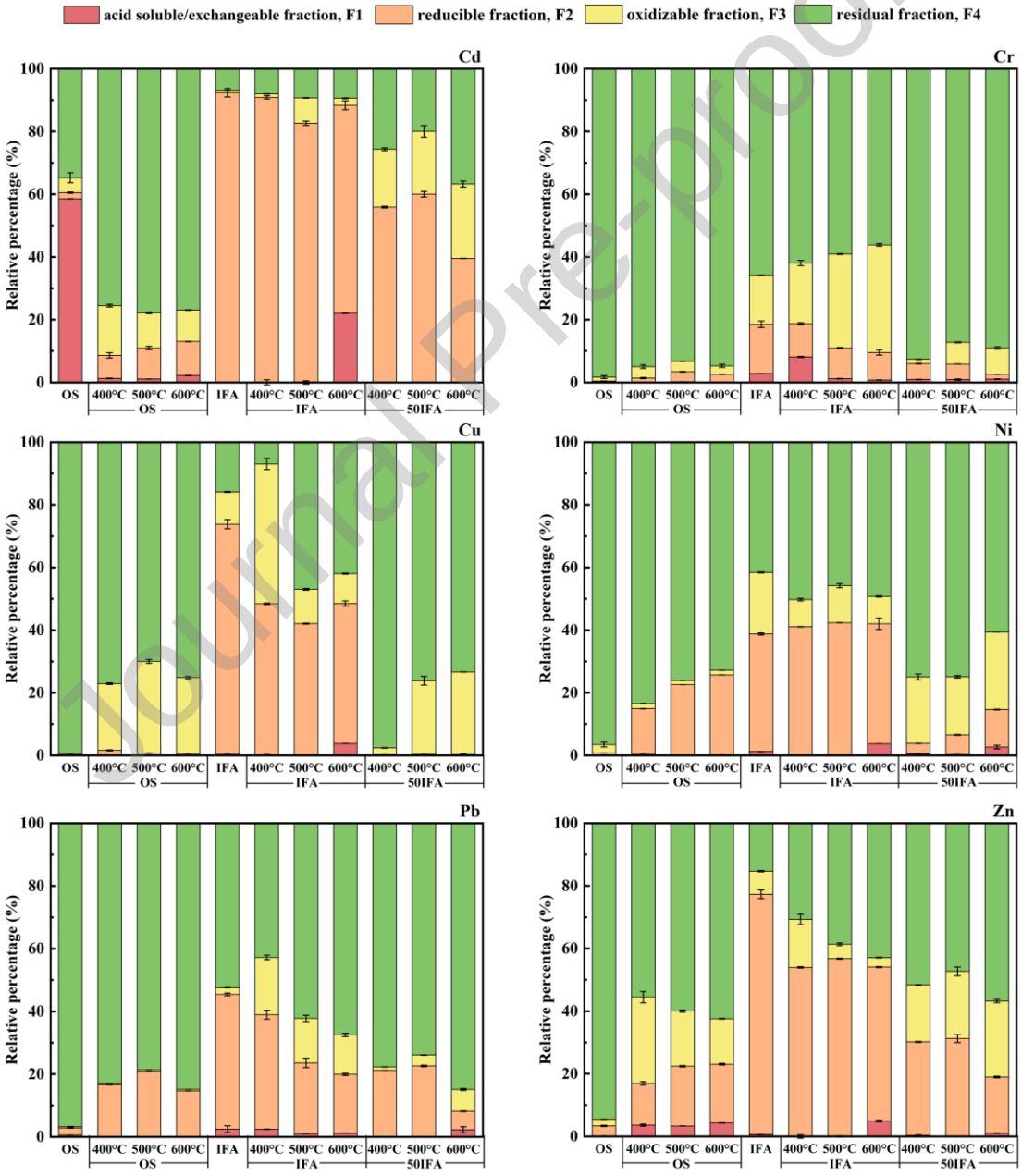

Fig. 6 Speciation distributions of Cd, Cr, Cu, Ni, Pb, and Zn in OS, IFA, and chars after pyrolysis at

different temperatures.

3.3.3 Environmental risk assessment of HMs

The potential ecological risk index (RI) was employed to evaluate the ecological risk of HMs in the pyrolysis chars as shown in Table S3 and Table 4. Notably, the C_f value of Cd in IFA was 13.65, manifesting high HM contamination. Moreover, the C_f values of Cu and Zn were 5.30 and 5.55, respectively, suggesting moderate contamination. Since the E_r value of IFA was 409.63, the RI value for IFA was 455.69, indicating a high level of comprehensive ecological risk. After IFA pyrolysis, the RI values of pyrolysis chars decreased but still exhibited high contamination levels. In contrast, the C_f value of Cd in OS (1.88) exhibited a low contamination, and the other HMs were within the clean risk level. The E_r value for Cd in OS was 56.38, suggesting moderate contamination. Overall, The RI value for OS was 56.25, suggesting a moderate comprehensive ecological risk. After OS pyrolysis, the E_r values of all HM elements were reduced to below 10, and the derived RI values of chars all indicate low risk levels. These results imply that individual pyrolysis is effective at stabilizing HMs in OS, while the effect is relatively weaker when applied to IFA.

After co-pyrolysis, the E_r values for Cd in the resulting chars significantly decreased, reaching a considerate level at 500°C (120.57) and a moderate level at 400°C and 600°C (91.81 and 51.66, respectively). Moreover, although the RI values for HMs in co-pyrolysis chars were higher than those in OS pyrolysis chars, a substantial reduction was observed when compared to the theoretical values, which still indicated high risks. This outcome demonstrates that the co-pyrolysis process effectively decreased the risk index of pyrolysis chars, especially for Cd. However, a potential environmental risk still exists due to the high HMs contamination in IFA.

Table 4 E_r and RI of the HMs in OS, IFA, and pyrolysis chars for the evaluation of ecological risk.

Item	E_r						E_r						RI	
	Cd	Cr	Cu	Ni	Pb	Zn	Cd	Cr	Cu	Ni	Pb	Zn		
OS	56.38	0.03	0.02	0.22	0.17	0.06	Moderate	Low	Low	Low	Low	Low	56.25	Moderate
OS-400	9.74	0.11	1.49	1.19	1.03	0.80	Low	Low	Low	Low	Low	Low	14.36	Low
OS-500	8.57	0.14	2.15	1.89	1.36	0.67	Low	Low	Low	Low	Low	Low	14.77	Low
OS-600	9.02	0.11	1.66	2.24	0.89	0.60	Low	Low	Low	Low	Low	Low	14.53	Low

IFA	409.63	1.04	26.51	8.44	4.54	5.55	Very high	Low		Low	Low	Low	455.69	High
IFA-400	344.99	1.23	67.18	5.94	6.69	2.26	Very high	Low	Moderate	Low	Low	Low	428.29	High
IFA-500	293.31	1.39	5.6 5	7.10	3.04	1.59	High	Low		Low	Low	Low	312.08	High
IFA-600	289.72	1.56	6.9 2	6.18	2.41	1.33	High	Low		Low	Low	Low	308.13	High
50IFA-400	87.14	0.16	0.1 2	2.01	1.43	0.94	Considerate	Low	Low	Low	Low	Low	91.81	Moderate
50IFA-500	120.57	0.29	1.5 7	2.01	1.77	1.11	Considerate	Low	Low	Low	Low	Low	127.33	Considerate
50IFA-600	51.66	0.25	1.8 2	3.90	0.74	0.76	Moderate	Low	Low	Low	Low	Low	59.12	Moderate
Theoretical E_r and RI values of pyrolysis chars after co-pyrolysis														
50IFA-400-theo	266.82	0.30	4.7 3	1.22	3.10	1.39	High	Low		Low	Low	Low	277.56	High
50IFA-500-theo	217.03	0.33	3.2 3	1.91	2.19	1.05	High	Low		Low	Low	Low	225.74	High
50IFA-600-theo	214.24	0.31	2.8 2	2.27	1.63	0.92	High	Low		Low	Low	Low	222.19	High

3.4 The mechanism of co-pyrolysis

To conclude the catalytic effect of IFA on OS pyrolysis and further investigate the synergistic effects of the co-pyrolysis process, FTIR and XRD were conducted to the chars.

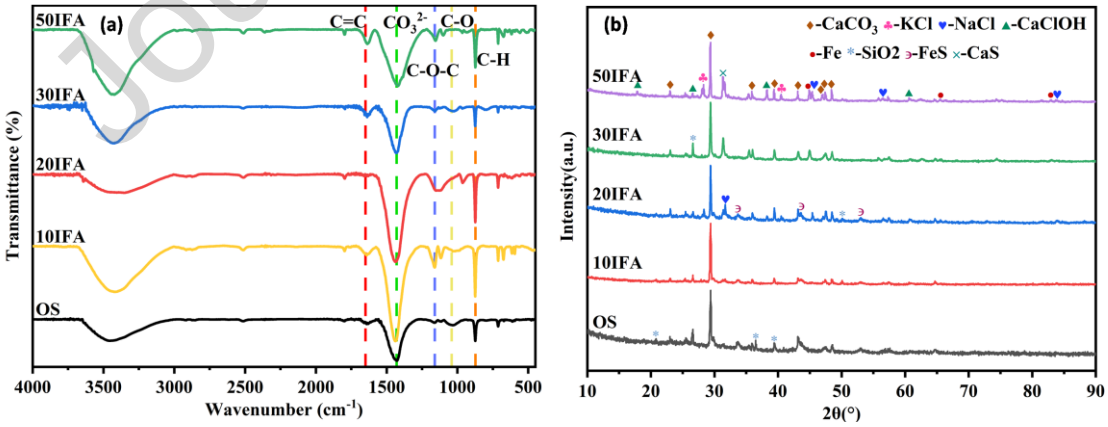

Fig. 7 (a) FTIR spectrum, and (b) XRD spectra of OS-600, 10IFA-600, 20IFA-600, 30IFA-600, 50IFA-600 chars.

3.4.1 Catalytic effect of IFA on OS pyrolysis

The functional groups presented in chars were analyzed using FTIR as depicted in Fig. 7(a). The variations in aromatic C=C (1640 cm^{-1}) [3] and C-H (874 cm^{-1}) [22, 24] bending vibrations exhibited a parallel trend with coke yield, affirming the accuracy of coke yield quantification. Moreover, the inverse relationship between the content of large PAHs in the pyrolysis oil (Fig. 4b) and the coke yield (Fig. 5a) further confirms that the addition of a moderate amount of IFA inhibited the poly-condensation of PAHs into coke precursor and promoted their cracking into light aromatic hydrocarbons [6, 9]. However, a higher addition ratio could weaken the chemical bond and enhance the chemical activity of hydrocarbon compounds in OS, leading to a higher accumulation of free radicals in chars [70] and then promoting coke formation with an increased aromatization degree in the char. The peak at 1034 cm^{-1}, which depicted C-O [47], was weakened in the chars with IFA addition, whereas the C-O-C peaks at 1158 cm^{-1} [5] were strengthened in 20IFA-600. This elucidates cations in IFA, such as Ca, may combine with oxygen-containing groups, leading to the formation of C-O-Ca or COO-Ca at a moderate addition ratio [17, 80]. Therefore, it can be inferred that Ca functioned as a cross-linking agent that immobilized macromolecular groups and prevented excessive condensation [17]. The strengthened calcite bending vibrations at 1428 cm^{-1} [54] confirmed the sequestration of emitted CO_2 in the pyrolysis char.

The plausible reaction pathways of co-pyrolysis are depicted in Fig. 8. Long-chain alkanes undergo cracking into light hydrocarbons, facilitated by the catalysis of CaO and chlorides presented in IFA [39, 46]. The resulting light hydrocarbons are further converted into MAHs and PAHs through aromatization reactions, potentially aided by active potassium species and $Ca(OH)_2$ [37]. The minerals in IFA may assist the side chain decomposition of aliphatic [68] and the hydrogenation of methylene in aromatic structure, leading to the formation of gaseous hydrocarbons. Furthermore, the strong basic nature of CaO and $Ca(OH)_2$ facilitates the catalytic deoxygenation of oxygenates, converting them into hydrocarbons, thereby promoting the formation of CO and CO_2 [27]. The observed decrease in CO content when IFA addition ratio exceeded 20 wt% confirms the enhanced water-gas shift reaction, and the adsorption of CO_2 by calcium-containing species further promoted it [12]. Particularly, heavy fractions in OS tend to undergo polycondensation and form coke at high temperatures, depositing on the char surfaces [44]. However, the minerals in IFA promotes their cracking [59] and then inhibits the formation of graphite structures in the aromatic carbon skeleton in char [6], ultimately resulting in the reduced coke yield and increased light aromatic hydrocarbons in pyrolysis oil.

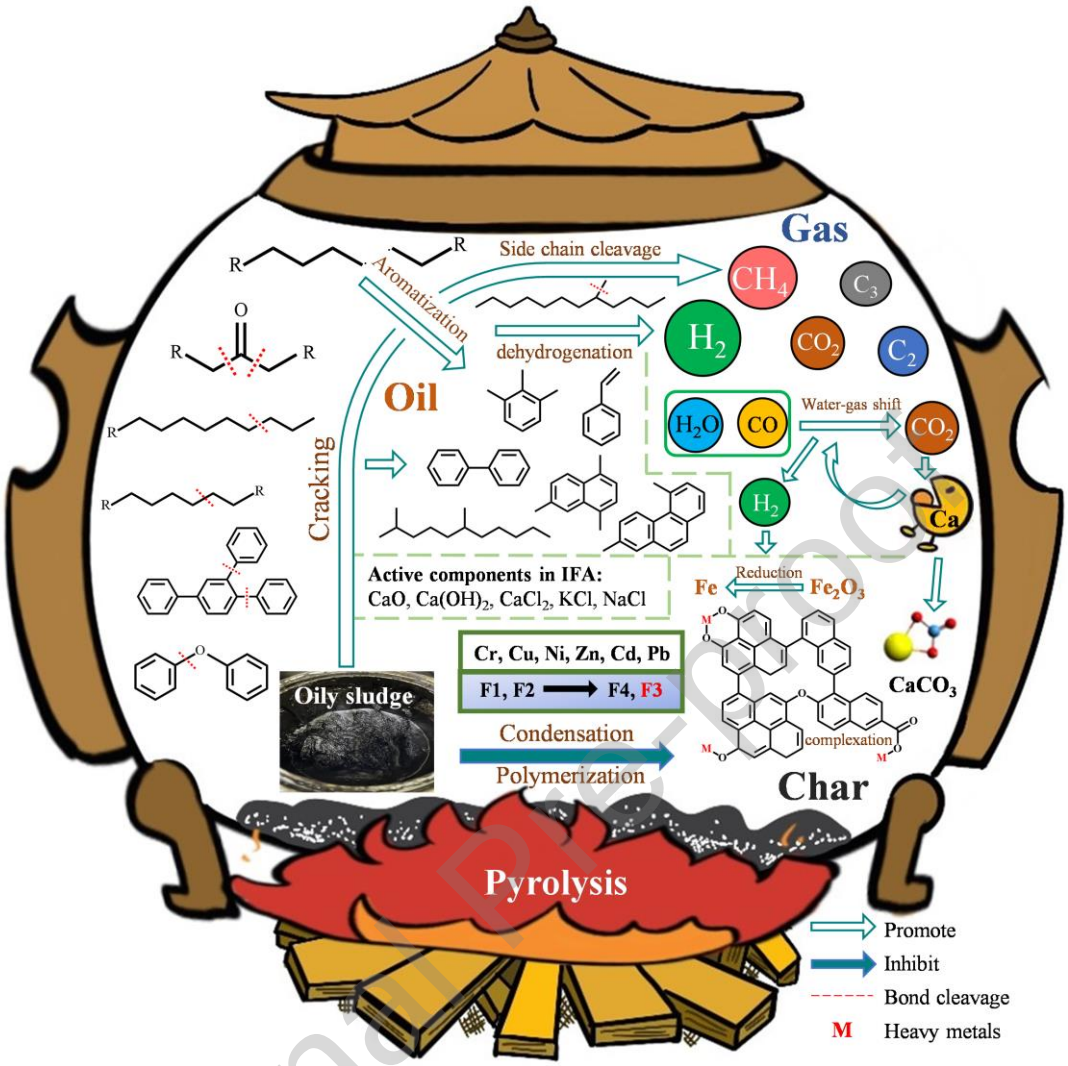

Fig. 8 Proposed mechanism of co-pyrolysis of OS with IFA.

3.4.2 Synergistic effects of co-pyrolysis

IFA addition induced the reduction reaction of inherent Fe species in OS. According to Fig. 7(b), metallic Fe peak was observed at 44.94°, 65.43°, and 82.90° in both 30IFA-600 and 50IFA-600 chars, while only ferrous iron was detected in OS char. The exclusive presence of Fe_2O_3 in the solid fraction of OS, as indicated in Fig. S1 (b), implies that the incorporation of IFA facilitated the reduction of Fe species derived from OS. This reduction reaction could be facilitated by the enhanced formation of H_2 and CO during co-pyrolysis and the involvement of Fe species in organic decomposition reactions. Therefore, the addition of IFA induced the in-situ catalysis of inherent reducible Fe species, and the lattice oxygen generated from its reduction can reduce the stability of heavy oil, leading to the formation of light oil fractions [15, 17, 40].

IFA addition reduces the concentration of CO_2 in derived pyrolysis gas, resulting in a higher flammability and making it a potential carbon capture and storage substrate. Fig. 7(b) illustrates the mineral compositions of pyrolysis chars. The increased peaks of $CaCO_3$, along with the occurrence of CaS, elucidate the adsorption of CO_2 and H_2S by IFA during the co-pyrolysis. The introduction of CaO and $Ca(OH)_2$ by IFA is crucial in adsorbing CO_2 generated during organic decomposition due to their high reactivity towards acidic gases [1, 50]. The increase of IFA addition leads to an enhanced CO_2 adsorption due to the higher content of Ca-bearing minerals, resulting in a significant low residual CO_2 content (0.60%) in the pyrolysis gas of 50IFA-600. Moreover, the heat generated during this reaction can be used to drive endothermic pyrolysis processes.

The results of leaching test and speciation distribution reveal the remarkable immobilization effect of co-pyrolysis on heavy metals in both IFA and OS, with a strong relationship to the pyrolysis temperature. In the case of IFA-600, the notable increase in the F1 fraction of Cd, Cu, Ni, and Zn can be attributed to the metal chlorides generated by the direct reactions between the chlorides and heavy metals [51, 73]. Subsequently, during co-pyrolysis, these metals were shifted from the active fractions to the F3 fraction with a notable rise comparing to theoretical values, which can be ascribed to the complexation of these metals originated from IFA with oxygen-containing functional groups on the char surface during co-pyrolysis [35, 36]. However, these functional groups were gradually decomposed at higher temperatures during OS individual pyrolysis, which lead to a slight decrease in F3 fractions of Cd and Zn. Wang et al. [64] also reported that higher pyrolysis temperature would result in increased aromatization degree of pyrolysis chars. Therefore, the abundant aromatic structures produced at higher temperatures may better immobilize HMs in the C matrix [35, 52], explaining the raised F3 fractions of Cd, Ni, Cu, and Zn in co-pyrolysis chars with elevated temperatures. Additionally, char densification during the pyrolysis, driven by organic compound decomposition, could concentrate Ni and Cu in the F3 fraction [69]. The shift from F4 to F2 and F1 for Ni in both OS pyrolysis chars and co-pyrolysis chars, observed with rising temperature, could be attributed to its catalytic role during pyrolysis. At higher temperatures, NiO might engage in Ni-catalyzed reactions [13], leading to changes in the metal speciation transformation. The presence of CaO and chlorides in IFA could potentially assist in HM fixation through facilitating the formation of stable metal oxides or crystal compounds during co-pyrolysis [66, 73]. This could explain the increased proportion of F4 fraction for Cd, Pb, and Zn after co-pyrolysis.

4. Conclusion

This study sheds light on the impact of IFA addition on product yields and compositions during the OS pyrolysis and reveals their interactions. The pyrolysis temperatures and mixing proportions were selected as parameters in the study. The results demonstrated that the highest oil yield, accompanied by the largest proportion of light oil, was obtained at a pyrolysis temperature of 600°C. The addition of IFA enhanced the water-gas shift and dehydrogenation reactions, resulting in a significant increase of H_2 yield from 21.02 L/kg OS to 60.95 L/kg OS when the IFA addition ratio increased from 0 to 50 wt%. The increased H_2 also converted the inherent Fe species in OS from a high-valence state to a low-valence state. Additionally, negligible CO_2 emission (0.59 L/kg OS) was observed in pyrolysis gas of 50IFA-600, with the generated CO_2 being efficiently sequestered within the pyrolysis char. Notably, adding a moderate content of IFA (e.g., 20wt%) presented the most significant impact on altering the composition of pyrolysis oil, resulting in the highest ratio of L/H. This effect was attributed to the aromatization of alkanes and the decomposition of large molecular PAHs, leading to a higher proportion of MAHs in the pyrolysis oil and reduced coke in the char. The gasoline yield also increased proportionally with the increased IFA addition ratio. Furthermore, the co-pyrolysis process effectively immobilized HMs in the char through complexation and embedding. The RI values were lowered from “very high” to “moderate” levels, indicating a reduced environmental risk.

Overall, the observed findings suggest that co-pyrolysis of OS with IFA is an effective approach for both value-added products recovery, CO_2 emission mitigation, and HM immobilization in the pyrolysis char. Experiments targeting the major catalytic components in IFA, encompassing both prominent minerals and trace elements, are essential to determine the mechanism of its comprehensive catalytic effect. Future research should also explore the potential application of the obtained pyrolysis oil and char.

CRediT authorship contribution statement

Di Yu: Experiment, Methodology, Investigation, Data curation, Software, Writing—original draft & revision. Zhiwei Li: Validation, Writing - review & editing. Jie Li: Writing - review & editing. Jun He: Writing - review & editing. Bo Li: Supervision, Writing - review & editing. Yin Wang: Conceptualization, Resources, Supervision, Project administration, Funding acquisition, Writing - review & editing.

Declaration of Competing Interest

The authors declare that they have no known competing financial interests or personal relationships that could have appeared to influence the work reported in this paper.

Acknowledgements

This work was supported by the Strategic Priority Research Program of the Chinese Academy of Sciences [Grant No. XDA23030301], the Alliance of International Science Organizations [Grant No. ANSO-CR-KP-2021-08], STS Plan Supporting Project of the Chinese Academy of Sciences in Fujian Province [Grant Nos. 2020T3036, 2021T3102, 2021T3073, 2021T3049, 2022T3065], and the Social Development Leading Key Projects of Fujian Province [Grant No. 2022Y0080,2021Y0069].

References

[1] Arias, B., A. Criado, Y., Pañeda, B., Abanades, J., 2022. Carbonation Kinetics of Ca $(OH)_2$ Under Conditions of Entrained Reactors to Capture CO_2. Industrial & engineering chemistry research 61(9), 3272-3277.

[2] Baig, J.A., Kazi, T.G., Arain, M.B., Shah, A.Q., Sarfraz, R.A., Afridi, H.I., Kandhro, G.A., Jamali, M.K., Khan, S., 2009. Arsenic fractionation in sediments of different origins using BCR sequential and single extraction methods. J Hazard Mater 167(1-3), 745-751.

[3] Ban, Y., Jin, L., Zhu, J., Liu, F., Hu, H., 2022. Insights into effect of Ca $(OH)_2$ on pyrolysis behaviors and products distribution of Hongshaquan coal. Fuel 307, 121791.

[4] Bisutti, I., Hilke, I., Raessler, M., 2004. Determination of total organic carbon–an overview of current methods. TrAC, Trends Anal Chem 23(10-11), 716-726.

[5] Cantrell, K.B., Hunt, P.G., Uchimiya, M., Novak, J.M., Ro, K.S., 2012. Impact of pyrolysis temperature and manure source on physicochemical characteristics of biochar. Bioresour Technol 107, 419-428.

[6] Chen, X., Liu, L., Zhang, L., Zhao, Y., Xing, C., Jiao, Z., Yang, C., Qiu, P., 2021. Effect of active alkali and alkaline earth metals on physicochemical properties and gasification reactivity of co-pyrolysis char from coal blended with corn stalks. Renewable Energy 171, 1213-1223.

[7] Chen, Z., Yu, G., Wang, Y., Wang, X., 2020. Fate of heavy metals during co-disposal of municipal solid waste incineration fly ash and sewage sludge by hydrothermal coupling pyrolysis process. Waste management 109, 28-37.

[8] Cheng, S., Takahashi, F., Gao, N., Yoshikawa, K., Li, A., 2016. Evaluation of oil sludge ash as a solid heat carrier in the pyrolysis process of oil sludge for oil production. Energy & Fuels 30(7), 5970-5979.

[9] Cheng, S., Wang, Y., Fumitake, T., Kouji, T., Li, A., Kunio, Y., 2017. Effect of steam and oil sludge ash additive on the products of oil sludge pyrolysis. Applied Energy 185, 146-157.

[10] Devi, P., Saroha, A.K., 2014. Risk analysis of pyrolyzed biochar made from paper mill effluent treatment plant sludge for bioavailability and eco-toxicity of heavy metals. Bioresour Technol 162, 308-315.

[11] Duan, Y., Gao, N., Sipra, A.T., Tong, K., Quan, C., 2022. Characterization of heavy metals and oil components in the products of oily sludge after hydrothermal treatment. Journal of Hazardous Materials 424, 127293.
[12] Gao, N., Li, J., Quan, C., Tan, H., 2020. Product property and environmental risk assessment of heavy metals during pyrolysis of oily sludge with fly ash additive. Fuel 266, 117090.
[13] Gao, N., Li, J., Quan, C., Wang, X., Yang, Y., 2020. Oily sludge catalytic pyrolysis combined with fine particle removal using a Ni-ceramic membrane. Fuel 277, 118134.
[14] Gong, Z., Du, A., Wang, Z., Fang, P., Li, X., 2017. Experimental study on pyrolysis characteristics of oil sludge with a tube furnace reactor. Energy & Fuels 31(8), 8102-8108.
[15] Gong, Z., Liu, C., Wang, M., Wang, Z., Li, X., 2020. Experimental study on catalytic pyrolysis of oil sludge under mild temperature. Sci Total Environ 708, 135039.
[16] He, D., Hu, H., Jiao, F., Zuo, W., Liu, C., Xie, H., Dong, L., Wang, X., 2023. Thermal separation of heavy metals from municipal solid waste incineration fly ash: A review. Chem Eng J, 143344.
[17] He, R., Deng, J., Deng, X., Xie, X., Li, Y., Yuan, S., 2022. Effects of alkali and alkaline earth metals of inherent minerals on Fe-catalyzed coal pyrolysis. Energy 238, 121985.
[18] Hu, G., Feng, H., He, P., Li, J., Hewage, K., Sadiq, R., 2020. Comparative life-cycle assessment of traditional and emerging oily sludge treatment approaches. Journal of Cleaner Production 251, 119594.
[19] Hu, G., Li, J., Zeng, G., 2013. Recent development in the treatment of oily sludge from petroleum industry: a review. J Hazard Mater 261, 470-490.
[20] Huang, Q., Han, X., Mao, F., Chi, Y., Yan, J., 2014. A model for predicting solid particle behavior in petroleum sludge during centrifugation. Fuel 117, 95-102.
[21] International, A., 2018. Standard Test Method for Water in Petroleum Products and Bituminous Materials by Distillation., ASTM D95-13.
[22] Jin, X., Teng, D., Fang, J., Liu, Y., Jiang, Z., Song, Y., Zhang, T., Siyal, A.A., Dai, J., Fu, J., 2021. Petroleum oil and products recovery from oily sludge: Characterization and analysis of pyrolysis products. Environ Res 202, 111675.
[23] Karamalidis, A.K., Voudrias, E.A., 2007. Release of Zn, Ni, Cu, SO42− and CrO42− as a function of pH from cement-based stabilized/solidified refinery oily sludge and ash from incineration of oily sludge. J Hazard Mater 141(3), 591-606.
[24] Keiluweit, M., Nico, P.S., Johnson, M.G., Kleber, M., 2010. Dynamic molecular structure of plant biomass-derived black carbon (biochar). Environmental science & technology 44(4), 1247-1253.
[25] Khachani, M., El Hamidi, A., Halim, M., Arsalane, S., 2014. Non-isothermal kinetic and thermodynamic studies of the dehydroxylation process of synthetic calcium hydroxide Ca $(OH)_2$. J. Mater. Environ. Sci 5(2), 615-624.
[26] Khaskhachikh, V., Gubina, N., Gerasimov, G., Kornilieva, V., 2019. Study of oil sludge pyrolysis in the presence of calcium oxide. Chemical Engineering Transactions 76, 1417-1422.
[27] Kumagai, S., Yamasaki, R., Kameda, T., Saito, Y., Watanabe, A., Watanabe, C., Teramae, N., Yoshioka, T., 2018. Aromatic hydrocarbon selectivity as a function of CaO basicity and aging during CaO-catalyzed PET pyrolysis using tandem μ-reactor-GC/MS. Chem Eng J 332, 169-173.
[28] Lai, D., Shi, Y., Geng, S., Chen, Z., Gao, S., Zhan, J.-H., Xu, G., 2016. Secondary reactions in oil shale pyrolysis by solid heat carrier in a moving bed with internals. Fuel 173, 138-145.
[29] Li, J., Li, L., Tong, Y.W., Wang, X., 2023. Understanding and optimizing the gasification of biomass waste with machine learning. Green Chemical Engineering 4(1), 123-133.
[30] Li, J., Lin, F., Li, K., Zheng, F., Yan, B., Che, L., Tian, W., Chen, G., Yoshikawa, K., 2021. A critical

review on energy recovery and non-hazardous disposal of oily sludge from petroleum industry by pyrolysis. J Hazard Mater 406, 124706.
[31] Li, J., Pan, L., Suvarna, M., Wang, X., 2021. Machine learning aided supercritical water gasification for H2-rich syngas production with process optimization and catalyst screening. Chem Eng J 426, 131285.
[32] Li, J., Suvarna, M., Pan, L., Zhao, Y., Wang, X., 2021. A hybrid data-driven and mechanistic modelling approach for hydrothermal gasification. Applied Energy 304, 117674.
[33] Li, J., Yu, G., Xie, S., Pan, L., Li, C., You, F., Wang, Y., 2018. Immobilization of heavy metals in ceramsite produced from sewage sludge biochar. Sci Total Environ 628, 131-140.
[34] Li, J., Zheng, F., Li, Q., Farooq, M.Z., Lin, F., Yuan, D., Yan, B., Song, Y., Chen, G., 2022. Effects of inherent minerals on oily sludge pyrolysis: Kinetics, products, and secondary pollutants. Chem Eng J 431, 133218.
[35] Li, Z., Yu, D., Wang, X., Liu, X., Xu, Z., Wang, Y., 2024. A novel strategy of tannery sludge disposal–converting into biochar and reusing for Cr (VI) removal from tannery wastewater. Journal of Environmental Sciences 138, 637-649.
[36] Liao, W., Zhang, X., Ke, S., Shao, J., Yang, H., Zhang, S., Chen, H., 2023. The influence of biomass species and pyrolysis temperature on carbon-retention ability and heavy metal adsorption property during biochar aging. Fuel Process Technol 240, 107580.
[37] Lin, B., Wang, J., Huang, Q., Chi, Y., 2017. Effects of potassium hydroxide on the catalytic pyrolysis of oily sludge for high-quality oil product. Fuel 200, 124-133.
[38] Lin, C., He, G., Li, X., Peng, L., Dong, C., Gu, S., Xiao, G., 2007. Freeze/thaw induced demulsification of water-in-oil emulsions with loosely packed droplets. Separation and purification technology 56(2), 175-183.
[39] Lin, F., Xiang, L., Sun, B., Li, J., Yan, B., He, X., Liu, G., Chen, G., 2021. Migration of chlorinated compounds on products quality and dioxins releasing during pyrolysis of oily sludge with high chlorine content. Fuel 306, 121744.
[40] Lin, F., Zheng, F., Li, J., Sun, B., Che, L., Yan, B., Chen, G., 2022. Catalytic pyrolysis of oily sludge with iron-containing waste for production of high-quality oil and H_2-rich gas. Fuel 326, 124995.
[41] Liu, J., Jiang, X., Zhou, L., Han, X., Cui, Z., 2009. Pyrolysis treatment of oil sludge and model-free kinetics analysis. Journal of hazardous materials 161(2-3), 1208-1215.
[42] Liu, J., Wang, Z., Xie, G., Li, Z., Fan, X., Zhang, W., Xing, F., Tang, L., Ren, J., 2022. Resource utilization of municipal solid waste incineration fly ash-cement and alkali-activated cementitious materials: A review. Science of The Total Environment, 158254.
[43] Liu, X., Yao, T., Lai, R., Xiu, J., Huang, L., Sun, S., Luo, Y., Song, Z., Zhang, Z., 2019. Recovery of crude oil from oily sludge in an oilfield by sophorolipid. Petroleum Science and Technology 37(13), 1582-1588.
[44] Liu, Y., Song, Y., Zhang, T., Jiang, Z., Siyal, A.A., Dai, J., Fu, J., Zhou, C., Wang, L., Li, X., 2021. Microwave-assisted pyrolysis of oily sludge from offshore oilfield for recovery of high-quality products. J Hazard Mater 420, 126578.
[45] Liu, Z., Fang, W., Cai, Z., Zhang, J., Yue, Y., Qian, G., 2022. Garbage-classification policy changes characteristics of municipal-solid-waste fly ash in China. Science of The Total Environment, 159299.
[46] Mahadevan, R., Adhikari, S., Shakya, R., Wang, K., Dayton, D., Lehrich, M., Taylor, S.E., 2016. Effect of alkali and alkaline earth metals on in-situ catalytic fast pyrolysis of lignocellulosic biomass: a microreactor study. Energy & Fuels 30(4), 3045-3056.
[47] Mo, W., Wu, Z., He, X., Qiang, W., Wei, B., Wei, X., Wu, Y., Fan, X., Ma, F., 2021. Functional group

characteristics and pyrolysis/combustion performance of fly ashes from Karamay oily sludge based on FT-IR and TG-DTG analyses. Fuel 296, 120669.
[48] Nelson, D.W., Sommers, L.E., 1996. Total carbon, organic carbon, and organic matter. Methods of soil analysis: Part 3 Chemical methods 5, 961-1010.
[49] Newsome, D.S., 1980. The water-gas shift reaction. Catalysis Reviews Science and Engineering 21(2), 275-318.
[50] Nikulshina, V., Gálvez, M., Steinfeld, A., 2007. Kinetic analysis of the carbonation reactions for the capture of CO2 from air via the Ca $(OH)_2$–$CaCO_3$–CaO solar thermochemical cycle. Chem Eng J 129(1-3), 75-83.
[51] Quan, C., Zhang, G., Gao, N., Su, S., Artioli, N., Feng, D., 2022. Behavior study of migration and transformation of heavy metals during oily sludge pyrolysis. Energy & Fuels 36(15), 8311-8322.
[52] Quan, C., Zhang, G., Xu, L., Wang, J., Gao, N., 2022. Improvement of the pyrolysis products of oily sludge: Catalysts and catalytic process. Journal of the Energy Institute.
[53] Ramaswamy, B., Kar, D., De, S., 2007. A study on recovery of oil from sludge containing oil using froth flotation. Journal of environmental management 85(1), 150-154.
[54] Reig, F.B., Adelantado, J.G., Moreno, M.M., 2002. FTIR quantitative analysis of calcium carbonate (calcite) and silica (quartz) mixtures using the constant ratio method. Application to geological samples. Talanta 58(4), 811-821.
[55] Roychand, R., De Silva, S., Setunge, S., Law, D., 2020. A quantitative study on the effect of nano SiO_2, nano Al_2O_3 and nano $CaCO_3$ on the physicochemical properties of very high volume fly ash cement composite. European Journal of Environmental and Civil Engineering 24(6), 724-739.
[56] Schumacher, B.A., 2002. Methods for the determination of total organic carbon (TOC) in soils and sediments. US Environmental Protection Agency, Office of Research and Development ….
[57] Shaheen, N., Jalil, A., Adnan, F., Arsalan Khushnood, R., 2021. Isolation of alkaliphilic calcifying bacteria and their feasibility for enhanced $CaCO_3$ precipitation in bio-based cementitious composites. Microbial Biotechnology 14(3), 1044-1059.
[58] Simoni, M., Hanein, T., Woo, C.L., Tyrer, M., Nyberg, M., Martinez, J.-C., Quintero-Mora, N.I., Provis, J.L., Kinoshita, H., 2022. Decarbonisation of calcium carbonate in sodium hydroxide solutions under ambient conditions: effect of residence time and mixing rates. Physical Chemistry Chemical Physics 24(26), 16125-16138.
[59] Sun, K., Themelis, N.J., Bourtsalas, A.T., Huang, Q., 2020. Selective production of aromatics from waste plastic pyrolysis by using sewage sludge derived char catalyst. Journal of Cleaner Production 268, 122038.
[60] Sun, S., Huang, X., Lin, J., Ma, R., Fang, L., Zhang, P., Qu, J., Zhang, X., Liu, Y., 2018. Study on the effects of catalysts on the immobilization efficiency and mechanism of heavy metals during the microwave pyrolysis of sludge. Waste Management 77, 131-139.
[61] Tang, Y., Chen, D., Feng, Y., Hu, Y., Yin, L., Qian, K., Yuan, G., Zhang, R., 2023. MSW pyrolysis volatiles' reforming by incineration fly ash for both pyrolysis products upgrading and fly ash stabilization. Chemosphere 313, 137536.
[62] Tian, Y., Li, J., Yan, X., Whitcombe, T., Thring, R., 2019. Co-pyrolysis of metal contaminated oily waste for oil recovery and heavy metal immobilization. J Hazard Mater 373, 1-10.
[63] Wang, F., Gao, N., Quan, C., Lai, X., 2022. Product distribution from oil sludge and waste tires under high pressure pyrolysis. Fuel 311, 122511.
[64] Wang, L., Xu, Y., Zhao, Z., Zhang, D., Lin, X., Ma, B., Zhang, H., 2022. Analysis of Pyrolysis

Characteristics of Oily Sludge in Different Regions and Environmental Risk Assessment of Heavy Metals in Pyrolysis Residue. ACS omega 7(30), 26265-26274.
[65] Wang, P., Hu, Y., Cheng, H., 2019. Municipal solid waste (MSW) incineration fly ash as an important source of heavy metal pollution in China. Environ Pollut 252, 461-475.
[66] Wang, X., Chang, V.W.-C., Li, Z., Song, Y., Li, C., Wang, Y., 2022. Co-pyrolysis of sewage sludge and food waste digestate to synergistically improve biochar characteristics and heavy metals immobilization. Waste Management 141, 231-239.
[67] Wang, X., Chi, Q., Liu, X., Wang, Y., 2019. Influence of pyrolysis temperature on characteristics and environmental risk of heavy metals in pyrolyzed biochar made from hydrothermally treated sewage sludge. Chemosphere 216, 698-706.
[68] Wang, Y., Li, Y., Wang, G., Wu, Y., Yang, H., Jin, L., Hu, S., Hu, H., 2022. Effect of Fe components in red mud on catalytic pyrolysis of low rank coal. Journal of the Energy Institute 100, 1-9.
[69] WD, C.U., Veksha, A., Giannis, A., Liang, Y.N., Lisak, G., Hu, X., Lim, T.-T., 2019. Insights into the speciation of heavy metals during pyrolysis of industrial sludge. Sci Total Environ 691, 232-242.
[70] Wu, B., Guo, X., Qian, X., Liu, B., 2022. Insight into the influence of calcium on the co-pyrolysis of coal and polystyrene. Fuel 329, 125471.
[71] Wu, Y., Wang, K., Wei, B., Yang, H., Jin, L., Hu, H., 2022. Pyrolysis behavior of low-density polyethylene over HZSM-5 via rapid infrared heating. Science of The Total Environment 806, 151287.
[72] Xia, Y., He, P., Shao, L., Zhang, H., 2017. Metal distribution characteristic of MSWI bottom ash in view of metal recovery. Journal of Environmental Sciences 52, 178-189.
[73] Xia, Y., Tang, Y., Shih, K., Li, B., 2020. Enhanced phosphorus availability and heavy metal removal by chlorination during sewage sludge pyrolysis. J Hazard Mater 382, 121110.
[74] Xu, N., Wang, W., Han, P., Lu, X., 2009. Effects of ultrasound on oily sludge deoiling. Journal of hazardous materials 171(1-3), 914-917.
[75] Xu, S., Hu, H., Guo, G., Gong, L., Liu, H., Yao, H., 2022. Investigation of properties change in the reacted molten salts after molten chlorides cyclic thermal treatment of toxic MSWI fly ash. Journal of Hazardous Materials 421, 126536.
[76] Yang, Y., Diao, R., Wang, C., Zhu, X., 2022. Co-pyrolytic interactions, kinetics and products of biomass pyrolysis coke and rapeseed cake: Machine learning, DAEM and 2D-COS analysis. Fuel 322, 124191.
[77] Yu, H., Li, J., Lin, F., Zeng, M., Li, R., Yan, B., Chen, G., 2023. Pyrolysis/combustion potential and heavy metal risk of oily sludge and derived products in industrial scale. Fuel 344, 128044.
[78] Zeng, X., Wang, Y., Yu, J., Wu, S., Zhong, M., Xu, S., Xu, G., 2011. Coal pyrolysis in a fluidized bed for adapting to a two-stage gasification process. Energy & fuels 25(3), 1092-1098.
[79] Zhang, Z., Gora-Marek, K., Watson, J.S., Tian, J., Ryder, M.R., Tarach, K.A., López-Pérez, L., Martínez-Triguero, J., Melián-Cabrera, I., 2019. Recovering waste plastics using shape-selective nano-scale reactors as catalysts. Nature Sustainability 2(1), 39-42.
[80] Zou, X., Yao, J., Yang, X., Song, W., Lin, W., 2007. Catalytic effects of metal chlorides on the pyrolysis of lignite. Energy & Fuels 21(2), 619-624.
[81] Zubaidy, E.A., Abouelnasr, D.M., 2010. Fuel recovery from waste oily sludge using solvent extraction. Process Safety and Environmental Protection 88(5), 318-326.

Declaration of Competing Interest

☒ The authors declare that they have no known competing financial interests or personal relationships that could have appeared to influence the work reported in this paper.

☐ The authors declare the following financial interests/personal relationships which may be considered as potential competing interests:

Graphical abstract

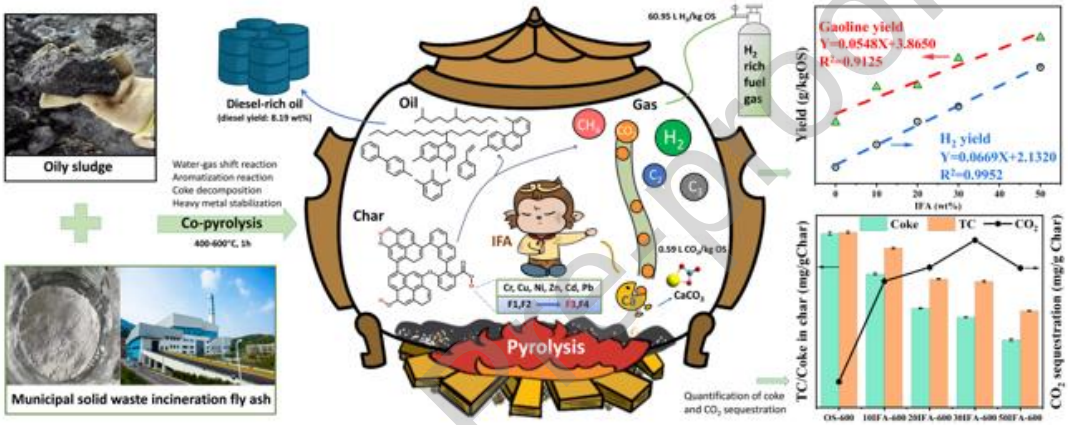

Environmental Implication

Oily sludge (OS) and incineration fly ash (IFA) are hazardous solid wastes that contain hydrocarbons, heavy metals, harmful microbes in OS, and heavy metals, dioxins, and furans in IFA. Improper disposal or treatment of these wastes can lead to soil and water contamination, posing a threat to the ecological environment. To address this issue, a co-pyrolysis approach was proposed to simultaneously treat these wastes, recover value-added products, and immobilize heavy metals in the char. This work provides a reference for synergistic treatment of OS and IFA and offers insights into the catalytic mechanism of a complex system.

Highlights

- A co-pyrolysis process of oily sludge and incineration fly ash is proposed.
- The addition of IFA can boost H_2 formation and CO_2 mitigation.
- Oil quality is significantly improved with moderate IFA addition.
- IFA curbs coke formation and encourages its decomposition into light aromatics.
- Co-pyrolysis significantly reduced the ecological risk of heavy metals in IFA.